Converged Dirac *R*-matrix calculation of electron impact excitation of Fe XVII

Guo-Xin Chen
ITAMP, Harvard-Smithsonian Center for Astrophysics, 60 Garden Street, Cambridge, Massachusetts 02138, USA
(Received 27 July 2007; revised manuscript received 21 September 2007; published 26 December 2007)

Large discrepancies exist between measurements [Brown *et al.*, Phys. Rev. Lett. **96**, 253201 (2006)] and previous calculations [Chen and Pradhan, Phys. Rev. Lett. **89**, 013202 (2002)] for electron impact excitation (EIE) cross sections in 3C (λ 15.015 Å) and 3D (λ 15.262 Å) of Fe XVII. A converged Dirac *R*-matrix calculation of EIE in Fe XVII with an accuracy of ≈5% (from theory estimate) in 3C and 3D cross sections is reported. We carry out five sets of Dirac *R*-matrix calculations to establish the convergence in our calculations. Full relativistic effects are included and the convergence of both the correlation and channel coupling effects and the combined effects of interacting Rydberg resonance series in EIE of Fe XVII is achieved. The intrinsic oscillatory features of 3C and 3D effective cross sections convolved with electron distributions are further demonstrated. Compared with recent electron beam ion trap (EBIT) measurements, there is still an ≈20% difference. I give one possible reason for this puzzling difference.

DOI: 10.1103/PhysRevA.76.062708 PACS number(s): 34.80.Kw, 52.70.La, 95.30.Ky

I. INTRODUCTION

Because of its closed *L*-shell ground electronic configuration, Fe XVII is the dominant Fe ion species in many laboratory and astrophysical plasmas [1–4]. Fe XVII is therefore important for spectral and abundance diagnostics in the x-ray region ~10–17 Å [5–10]. X-ray line strengths and ratios of spectral line intensities in Fe XVII can be used as a fundamental diagnostic tool to reveal the nature of astrophysical sources, such as high-temperature stellar coronae and accretion disks around active galactic nuclei [11–13], given that the line formation mechanisms in Fe XVII are well-studied and can be accurately modeled [6,8,14]. For these reasons, there has been a rich theoretical and experimental study of fundamental atomic processes in Fe XVII atomic and spectral systems over the past several decades (e.g., [7–9,14]). But the diagnostic capabilities of Fe XVII are still limited and the line-formation mechanisms in the Fe XVII x-ray spectra have not yet been fully understood. One latest evidence is reflected from the large discrepancies (up to 50% or more) in electron impact excitation (EIE) cross sections of the Fe XVII x-ray transitions 3C (λ 15.015 Å, $2p^5 3d\ ^1P_1^o \rightarrow 2p^6\ ^1S_0$) and 3D (λ 15.262 Å, $2p^5 3d\ ^3D_1^o \rightarrow 2p^6\ ^1S_0$) between measurements [14] and previous calculations (e.g., [8]). Indeed this is only one among a series of unresolved long-standing problems in Fe XVII atomic and spectral systems [6,7,9].

The determination of accurate EIE cross sections in Fe XVII plays a cornerstone role in the field of x-ray astrophysics [3,7–10,14]. On the theoretical perspective, accurate EIE calculation for Fe XVII is notoriously difficult. The distorted wave or relativistic distorted wave (RDW) method with and without the inclusion of resonance effects in the isolated-resonance approximation was commonly used in previous calculations (e.g., [3,15]). Only limited success was achieved, however, and these calculations are not accurate enough for applications [4,7,14]. We have also carried out a Breit-Pauli *R*-matrix (BPRM) calculation [8,16] including Rydberg resonances for target states up to the principal quantum number $n=4$. A number of results were reported which have general impact on the EBIT science and x-ray astronomy. The line ratios 3C/3D based on this calculation are in agreement with EBIT experiments at low electron beam energies. However, the story of Fe XVII atomic calculations was not complete in this study either because the convergence of the resonance effects and the correlation and collisional (or channel) coupling effects in the scattering calculation was not investigated. It is interesting that our BPRM calculation was later confirmed by $n=4$ and $n=5$ Dirac *R*-matrix (DRM) calculations [17,18], indicating the *same* limitations in all these calculations. A semiempirical approach has also been applied to the calculation of 3C/3D line ratios for a range of Ne-like ions [19].

On the experimental perspective, electron beam ion trap (EBIT) has been used to measure the 3C and 3D spectrum [7,14], which may be used to derive 3C and 3D effective cross sections. Brown *et al.* in [14] argue that they have established a benchmark for atomic calculations of Fe XVII. The method they used is to derive the "absolute" EIE cross sections of Fe XVII from the x-ray spectrum measured on EBIT. They used a microcalorimeter instrument on EBIT to measure the spectrum of weak radiative recombination (RR) lines to Fe XVI. They derived the 3C and 3D EIE cross sections of Fe XVII when normalizing their spectrum to the weak RR spectrum (with cross sections over three orders of magnitude smaller than the direct excitation transitions).

The accuracy of EBIT spectrum measurements was reported to be at a level of 10% (1σ standard error). However, Fe XVII is such a complex atomic system that the accurate atomic calculation has proven to be challenging. In order to meet the theoretical and EBIT experimental challenges (5–10 % accuracy in 3C and 3D EIE cross sections), in this work I report a fully relativistic *R*-matrix calculation of EIE of Fe XVII. The convergence of both the correlation and channel coupling effects and the combined resonance effects in EIE of Fe XVII is studied. The GRASP2 code [20] and the Dirac *R*-matrix (DRM) codes DARC [21] with slight modifications are used for calculations of Fe XVII atomic structure and collisional dynamics.

II. METHOD

I use the N- and $(N+1)$-electron Dirac-Coulomb (DC) Hamiltonian (N is the number of electrons) to describe the target and the collisional atomic system, respectively. The DC Hamiltonian for electrons i and i' in a central field Z (atomic number $Z=26$ for Fe XVII) is

$$H^{\mathrm{DC}} = \sum_{i=1} \left(\boldsymbol{\alpha} \cdot \boldsymbol{p}_i / \alpha + \beta / \alpha^2 - \frac{2Z}{r_i} + \sum_{i'>i} \frac{2}{r_{ii'}} \right) \quad (2.1)$$

(in Rydberg units); the quantities $\boldsymbol{\alpha}$ and β are the Dirac matrices in the low-energy representation, and α is the fine-structure constant. The total wave functions for a given symmetry $J\pi$ (J is the total angular momentum in a jj-coupling scheme and π is the parity) are constructed from bound and free Dirac four-component spinors.

The Fe XVII target wave functions including up to principal quantum number $n=5$ and relativistic angular quantum number $|\kappa|$ up to 4 (or the total angular momentum j up to 7/2) for the singly excited electron from the $2s$ or $2p$ subshell, are calculated using the multiconfiguration Dirac-Fock (MCDF) method [N-electron DC Hamiltonian in Eq. (2.1)]. For a target so specified, electron collision processes are represented by a partial-wave (PW) expansion with radial functions satisfying the $(N+1)$-electron DC Hamiltonian in Eq. (2.1), leading to close-coupling (CC) solutions. Using the PW approach for the colliding electron, the coupled-channel wave function expansion for the (e+Fe XVII) system may be expressed as

$$\Psi(E; e + \mathrm{Fe\ XVII}) = \sum_i \chi_i(\mathrm{Fe\ XVII})\theta_{e,i}(\kappa) + \sum_j c_j \Phi_j(\mathrm{Fe\ XVI}), \quad (2.2)$$

where Ψ denotes the continuum ($E>0$) states of a given symmetry $J\pi$, expanded in terms of the core ion eigenfunctions χ_i(Fe XVII) with a specific total angular momentum and parity combination $J_\iota \pi_\iota$ of the target, and the PW $\theta_{e,i}(\kappa)$ for the colliding electron $(N+1)$ (with relativistic quantum number κ_ι) in a channel labeled $J_\iota \pi_\iota\ k_\iota \kappa_\iota [J\pi]$; k_ι^2 is the channel energy in Rydberg (<0 if closed). I consider symmetries with $2J \leq 61$ to ensure the PW convergence at low energies for both parities explicitly in the DRM calculations. The variationally added functions Φ_j(Fe XVI), sometimes referred to as "bound channels" as opposed to the continuum or "free" channels in the first sum over the target states, form a set of L^2-integrable antisymmetrized wave functions. The DRM method is used to find the unknown continuum radial functions $\theta_{e,i}(\kappa)$ and CC expansion coefficients c_j in Eq. (2.2). The continuum states satisfy certain boundary conditions. In Eq. (2.2), both spectroscopic orbitals and pseudo-orbitals may be included. Pseudo-orbitals may be needed for a converged calculation to incorporate the major part of the residual long-range interelectron Coulomb interactions as reflected in the long-range channel coupling and correlation effects, and the short-range exchange and correlation effects.

III. CALCULATION

In this work, I carry out five sets of DRM calculations for three reasons: (a) To show the influence of long-range channel coupling and correlation effects and short-range exchange effects; (b) to demonstrate the intrinsic oscillatory features in 3C and 3D averaged collision strengths or effective cross sections; (c) to carry out *consistent* calculations using the same computer packages to elucidate previous similar calculations and to make a more meaningful comparison among them. In the first calculation (A) (referred to mode $n=3$ below), target states up to $n=3$ in $2s^2 2p^6$ and $2s^2 2p^5 3\ell$ ($\ell = s,p,d$) are included. In the second calculation (B) (mode $n=4$), in addition to (A), I include $2s^1 2p^6 3\ell$ ($\ell = s,p,d$) and $2s^2 2p^5 4\ell$ ($\ell = s,p,d,f$). In the third calculation (C) (mode $n=5$), I add $2s^2 2p^5 5\ell$ ($\ell = s,p,d,f$) to (B). In the fourth calculation (D) (mode $n=5+$), in addition to those states in (C), I include target states in $2s^2 2p^4 3d^2$ to reflect the pair excitation effects from the ground state $2s^2 2p^6$; I also include pseudo-orbitals with the relativistic angular quantum number $|\kappa| = 1-3$ to incorporate short-range exchange and correlation effects and long-range channel coupling and correlation effects. To show the convergence of calculation (D), I also carry out the fifth calculation (E) (mode $n=4+$), adding those pair excitation states and pseudo-orbitals mentioned in (D) to (B). The radiation damping effect is included in mode $n=5+$ but it is found to be negligibly small for 3C and 3D. The present calculation modes (A)–(C) should be respectively comparable to (i) the $n=3$ term-coupling R-matrix calculation [22], (ii) our previous $n=4$ BPRM calculation [8] and the $n=4$ DRM calculation [17], and (iii) the $n=5$ DRM calculation [18].

IV. RESULT

A. Detailed and averaged collision strength

The detailed collision strengths Ω of 3C and 3D as a function of electron impact energy E from mode $n=5+$ are shown in Fig. 1. The combined resonance effects of interacting Rydberg resonance series in 3C and 3D are clearly demonstrated. The combined resonance effects, which include the Rydberg resonance series and their mutual interactions and their constructive and destructive interference with the background (i.e., direct EIE scattering), may be readily calculated using the R-matrix method as employed in the present work. These Ω form the basis below to compute averaged collision strengths $\bar{\Omega}$ for convergence demonstration and effective cross sections $\bar{\sigma}$ for comparisons with cross sections derived from EBIT [14] and previous calculations.

To show the convergence of my calculations, I define averaged collision strength $\bar{\Omega}$,

$$\bar{\Omega} = \frac{\int \Omega(E) g(E) dE}{\int g(E) dE}, \quad (4.1)$$

where $g(E)$ is the electron distribution function (assumed to be a Gaussian beam distribution for EBIT). In Fig. 2, I show

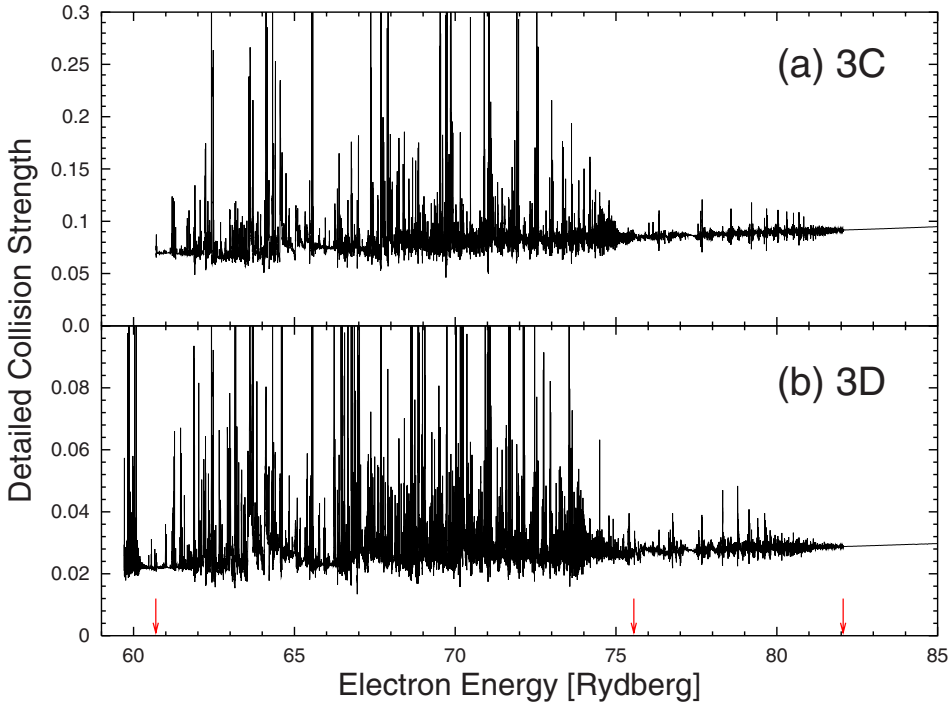

FIG. 1. (Color online) Detailed fine-structure collision strengths Ω (mode $n=5+$) as a function of incident electron energy E for 3C [top panel (a)] and 3D [bottom panel (b)]. The arrows from left mark the highest target thresholds (included in DRM calculation) of $n=3$, 4, and 5, respectively.

$\bar{\Omega}$ calculated with Eq. (4.3) from their respective Ω in modes (A)–(E) [see Fig. 1 for (D) mode $n=5+$]. FWHM (full width at half maximum) $W=20$ eV is used in all the curves of Fig. 2 except the red ones. At low energy, strong resonance effects on 3D $\bar{\Omega}$ are shown. The resonance effects on 3C $\bar{\Omega}$ are small but discernible for $W=20$ eV. The red curves are for $W=10$ eV calculation in mode $n=5+$. The intrinsic oscillation features of $\bar{\Omega}$ for both 3C and 3D are demonstrated. In $E=62-66$ Ry region, the effects of Rydberg resonance series are up to 7% ($W=20$ eV) and 11% ($W=10$ eV) for 3C; 25% ($W=20$ eV) and 33% ($W=10$ eV) for 3D. The importance of resonance effects are clearly demonstrated for 3D and to a less extent for 3C. This supports the conclusion given in our earlier BPRM calculation [8]. The results of modes $n=4+$ and 5+ are converged, so the calculation of mode $n=4+$ is not shown in Fig. 2. The results of mode $n=4+$ are given in Table I below. In Fig. 2(a), from the comparison between curves of mode $n=5+$ and other curves, I show that it is important to include the pair excitation states and the long-range correlation and collisional coupling effects for 3C. Because of the competition of these effects mainly from the correlation effects in the target and from the collisional coupling effects, these combined effects are relatively small for 3D.

B. Effective cross section

In EBIT measurements, the line intensity may be expressed as [7,8,14]

$$I = \eta \int g(E) v_e dE \, \bar{\sigma} n_e n_{\mathrm{Fe\ XVII}}, \tag{4.2}$$

where n_e and $n_{\mathrm{Fe\ XVII}}$ are the electron density and the Fe XVII ion density, respectively. η is the combined correction coefficient for the detector. v_e is the velocity of the incident electron. The effective EIE cross section $\bar{\sigma}$ is defined as

$$\bar{\sigma} = \frac{\int \sigma(E) g(E) v_e dE}{\int g(E) v_e dE}. \tag{4.3}$$

Here the detailed cross sections σ is calculated from the detailed Ω,

$$\sigma = \frac{\pi a_0^2}{w k^2} \Omega, \tag{4.4}$$

where k is the relativistic wave quantum number and $k^2 = E(1+\alpha^2 E/4)$; a_0 is the Bohr radius and w is the statistical weight of the initial transition state.

In Table I, we compare the effective cross sections defined in Eq. (4.3) among the present calculations with different modes, and the previous theory and experiment results. The results of mode $n=3$ should be comparable to those in [22]. The RDW results [15] without resonances and cascades are also similar to mode $n=3$ results as evidenced from Table I. The lack of Rydberg series of resonances and other limitations in mode $n=3$ or in [22] have been discussed in [8]. The results of modes $n=4$ and $n=5$ should be comparable to those in [8,17] and in [18], respectively. While to a large extent the combined effects of interacting Rydberg resonance series are included in these $n=4$ and 5 calculation modes, the convergence of correlation and channel coupling effects was *not* achieved in all of them. From Fig. 2 and Table I, we find that both (a) the combined effects of interacting Rydberg resonance series and (b) the effects of the convergence of correlation and collisional coupling are achieved in modes $n=4+$ and 5+. For 3C, the effective cross sections $\bar{\sigma}$ from

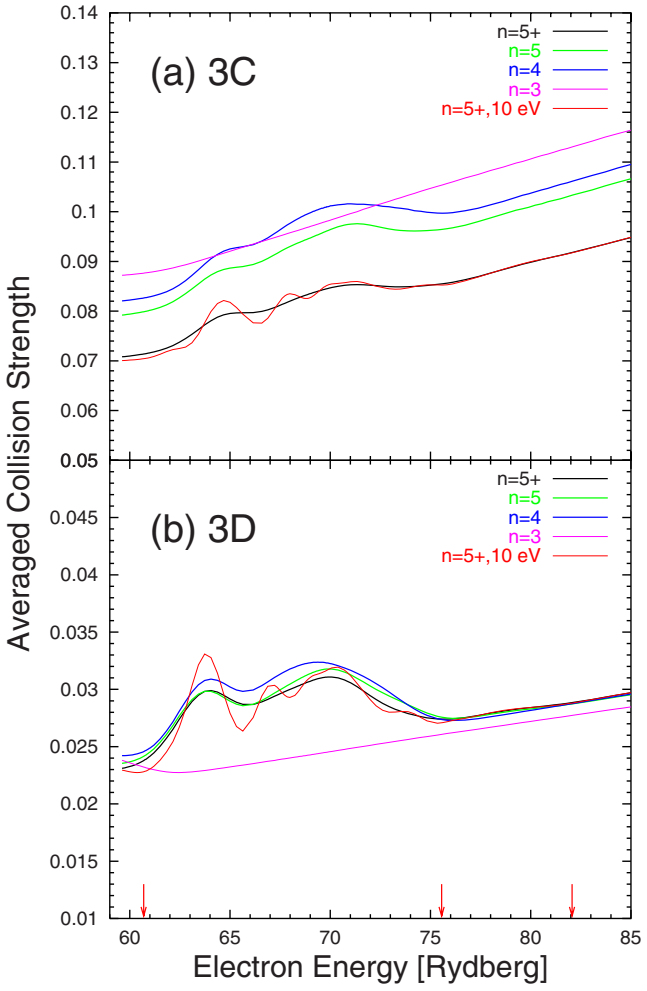

FIG. 2. (Color online) Averaged collision strengths $\bar{\Omega}$ as a function of incident electron energy E for 3C [top panel (a)] and 3D [bottom panel (b)]: Black (mode $n=5+$, $W=20$ eV); green (mode $n=5$, $W=20$ eV) (thick gray in black and white printing); blue (mode $n=4$, $W=20$ eV) (thick black); orange (mode $n=3$, $W=20$ eV) (thin gray); red (mode $n=5+$, $W=10$ eV) (thin black). The curve of mode $n=5+$ and $W=10$ eV oscillates along the curve of mode $n=5+$ and $W=20$ eV.

mode $n=5+$ (seventh column) are 12–14 % smaller than those from mode $n=5$ (fifth column); for 3D, the $\bar{\sigma}$ of mode $n=5+$ are only up to 3% smaller than the $\bar{\sigma}$ of mode $n=5$ due to the competition between the target correlation and the collisional coupling effects as explained above. In order to compare with EBIT results, it is more meaningful to use mode $n=5++$, where cascade effects are added to mode $n=5+$.

The present results of mode $n=5++$ are about 10% smaller than RDW calculations in [14] for 3D, and about 20% smaller for 3C. Both mode $n=5++$ results and RDW calculations in [14] include the resonance and cascade effects. However, as we pointed out before [8], the RDW method may not be accurate enough (in contrast to the relativistic close coupling method) in particular for treating interacting Rydberg series of resonances. The present results of mode $n=5++$ are about 25% (910 eV) and 20% (964 eV) larger than the EBIT derived 3C data in [14] (last column), and 24% (910 eV) and 31% (964 eV) larger for 3D. It is remarkable that the difference at 964 eV for 3D is much larger than for 3C. The percentage difference between the present converged 3C and 3D effective cross sections and the EBIT derived data in [14] is now uniformly within 20–30 %. One possible reason for this 20–30 % difference may be that the theory recombination rates used for normalization in [14] are not so accurate [23].

C. Maxwellian-averaged effective collision strength

I compare the present 3C and 3D Maxwellian-averaged effective collision strengths with previous calculations in Table II for temperatures between 2 MK (1 MK=10^6 K) and 10 MK. The Maxwellian-averaged effective collision strength is defined as

$$\Upsilon(T) = \int_{\Delta E}^{\infty} \Omega(E) \exp\left(-\frac{E}{kT}\right) d\left(\frac{E}{kT}\right), \tag{4.5}$$

for a Maxwellian electron distribution function with temperature T. ΔE is the excitation energy between the initial and final states. The quantity $\Upsilon(T)$ is widely used in thermalized plasmas appearing in various terrestrial and space sources.

From the comparison of $\Upsilon(T)$ in Table II, we again find that the present mode $n=4$ and $n=5$ data are in good agreement with our previous $n=4$ BPRM results [8] and previous $n=5$ results of [18]. In fact, the $n=5$ calculations show no improvement at $T \geq 4$ MK and only a marginal improvement at lower T over the $n=4$ $\Upsilon(T)$ data. The $\Upsilon(T)$ difference between the present $n=4$ mode and our previous $n=4$ BPRM calculation is up to 3% for 3C and up to 5% for 3D. This comparison more or less shows the full relativistic effect in target and collisional dynamics (beyond the BPRM level) that is in included in the present work. Our mode $n=4+$ and $n=5+$ results are also converged, with significant improve-

TABLE I. Effective cross sections $\bar{\sigma}$ (in units 10^{-19} cm^2=0.1 Mb) for 3C and 3D from the present calculations (with $W=20$ eV) are compared with previous results.

	E(eV)	Present calc.						Previous calc.		Expt.
		$n=3$	4	5	4+	5+	5++	[15]	[14]	[14]
3C	910	1.24	1.25	1.19	1.08	1.06	1.06	1.21	1.26	0.849±0.16
	964	1.23	1.26	1.21	1.08	1.06	1.07	1.19	1.30	0.888±0.93
3D	910	0.312	0.403	0.385	0.394	0.383	0.384	0.319	0.417	0.310±0.64
	964	0.308	0.394	0.390	0.385	0.381	0.391	0.314	0.437	0.298±0.33

TABLE II. Maxwellian-averaged effective collision strength $\Upsilon(T)$ for 3C and 3D from the present *R*-matrix calculations are compared with previous *R*-matrix results.

	T	Present calc.				Previous calc.	
		$n=4$	5	4+	5+	[8]	[18]
3C	2 MK	0.0992	0.0958	0.0855	0.0850	0.102	0.0957
	4 MK	0.112	0.108	0.0964	0.0960	0.112	
	5 MK	0.117	0.114	0.102	0.101	0.117	0.114
	10 MK	0.143	0.140	0.125	0.125	0.143	0.140
3D	2 MK	0.0294	0.0289	0.0288	0.0287	0.0279	0.0290
	4 MK	0.0316	0.0313	0.0312	0.0312	0.0302	
	5 MK	0.0327	0.0325	0.0325	0.0325	0.0316	0.0325
	10 MK	0.0386	0.0386	0.0388	0.0389	0.0400	0.0385

ments (at least 13 % smaller) over all the other calculations for 3C. However, the combined effects on 3D $\Upsilon(T)$ data is less than 1%, although the 3D *A* coefficients from modes $n=4+$ and $n=5+$ are 4% higher (see Sec. IV D below). These comparisons confirm the conclusion obtained in the previous subsections, and thus establish the overall convergence either between the present calculations or between the present and previous calculations if the same computation modes are employed.

D. Transition probability

Finally, in order to gauge the convergence in the target calculations, in Table III, I compare transition probabilities *A* in length form from the present five calculation modes, our previous calculation in [8], the previous calculation in [18], and NIST recommended *A* coefficients [24] for 3C and 3D. N.B. NIST 3C and 3D *A* coefficients are also from theory.

From the comparison of Table III, we find that the *A* coefficients from the present mode $n=4+$ and $n=5+$ calculations are converged, with significant improvements over all the other modes in this work and previous results in [8] and [18], for both 3C and 3D. The present converged 3C and 3D *A* coefficients (from modes $n=4+$ and $n=5+$) are 9% smaller than the present mode $n=5$ or previous $n=5$ data in [18], while the present converged 3D *A* coefficient is 4% higher. We find that the percentage differences are significantly different between this comparison of *A* coefficients and previous comparisons of collision strengths or cross sections. For example, in our comparison above in Table I, the $\bar{\sigma}$ percentage difference between modes $n=5+$ and $n=4+$ is up to 5% *larger* for 3C and 5% *smaller* for 3D than the respective *A*-coefficient percentage difference between the two modes. This shows that collisional coupling plays a significant role in the accurate calculations of 3C and 3D cross sections. This conclusion in turn indicates that collisional coupling plays a significant role in the accurate determination of the individual 3C and 3D line emissivities or the resulting 3C/3D line ratios in real plasmas when a collisional-radiative model is employed.

V. DISCUSSION AND SUMMARY

In summary, the major results I have achieved are as follows.

(1) A converged Dirac *R*-matrix calculation is carried out for EIE of Fe XVII. Both the combined effects of interacting Rydberg resonance series and the effects of long-range correlation and channel coupling are demonstrated to be important in EIE calculations of Fe XVII. The calculations of both the target structure and the collisional dynamics are demonstrated to converge to within $\approx 5\%$.

(2) The five calculation modes in the present work convincingly elucidate the convergence of some important effects such as resonance, correlation, and collisional or channel coupling. These five calculation modes are carried out with the same computer package, so this work is particularly useful in order to elucidate or compare to our previous *R*-matrix calculation and several other previous *R*-matrix calculations from different sources. The consistency between the present *R*-matrix calculation and the previous *R*-matrix calculations is demonstrated when the same computation mode is used.

(3) Compared to target calculations used in the previous *R*-matrix work, the *A* coefficients in the present converged target calculation are 9% smaller for 3C and 4% *larger* for

TABLE III. Transition probabilities *A* (in units 10^{13} s^{-1}) in length form for 3C and 3D from the present calculations are compared with previous results and NIST recommended data.

			Present calc.		Previous calc.		NIST
	$n=4$	5	4+	5+	[8]	[18]	[24]
3C	2.50	2.45	2.25	2.25	2.59	2.46	2.28
3D	0.592	0.610	0.631	0.635	0.562	0.609	0.600

3D. Compared to $n=5$ mode, the effective cross sections in $n=5+$ mode (with the inclusion of pseudostates and pair excitations) are 12–14 % smaller for 3C and up to 3% *smaller* for 3D. The full relativistic effect beyond our previous BPRM work results in a difference of up to 3–5 % in effective cross sections or collision strengths. Compared to the $n=4$ Maxwellian-averaged effective collision strengths $\Upsilon(T)$ data, the $n=5$ calculations of $\Upsilon(T)$ show no improvement for temperature $T \geq 4$ MK and only a marginal improvement at lower T.

(4) The present results reduce significantly from the difference of up to 50% to 20–30 % between the reported 3C and 3D effective cross sections derived from EBIT spectrum in [14] and previous calculations. This difference of 20–30 % is now systematic (instead of random as appeared in other calculations) for both 3C and 3D. The present 3C and 3D effective cross sections are shown to converge to within 5% (theoretical estimate). Therefore, one possible reason for the 20–30 % difference between the present converged effective cross section and those derived from EBIT spectrum in [14] may be that the theory recombination rates used for normalization in [14] are not so accurate.

(5) The convolution of 3C and 3D cross sections with different electron beam distributions reveals the intrinsic oscillatory features. The effective cross sections should also depend sensitively on beam widths.

(6) The results obtained and the method used in this paper should have a general impact on the calculations of EIE and other fundamental atomic processes. A systematic calculation of Ne isoelectronic sequence and other ions is currently underway.

With this sophisticated and accurate calculation (and other calculations by the present author), a systematic study of x-ray spectral diagnostics and modeling via an extensive and elaborate collisional-radiative model is also currently underway for immediate application to EBIT measurements as well as astrophysical, fusion, and laser-produced plasmas.

ACKNOWLEDGMENTS

The author would like to thank our EBIT team members based at NIST and CfA for stimulating discussions and thank J. C. Raymond at CfA for beneficial conversations. M. Pindzola and C. Ballance sent a copy of tabulated 3C and 3D cross sections used for a plot in their published paper. The author is also grateful for K. Kirby and N.S. Brickhouse's encouragement of the project. This work was supported by NSF through a grant for the Institute for Theoretical Atomic, Molecular and Optical Physics at Harvard University and Smithsonian Astrophysical Observatory and in part by a Chandra X-ray Observatory (CXO) theory grant. All the computational work was carried out on the Cluster at the Computation Facility of CfA.

[1] M. D. Rosen *et al.*, Phys. Rev. Lett. **54**, 106 (1985); D.L. Matthews *et al.*, *ibid.* **54**, 110 (1985).
[2] R. E. Marrs, M. A. Levine, D. A. Knapp, and J. R. Henderson, Phys. Rev. Lett. **60**, 1715 (1988).
[3] B. W. Smith, J. C. Raymond, J. B. Mann, and R. D. Cowan, Astrophys. J. **298**, 898 (1985).
[4] C. R. Canizares *et al.*, Astrophys. J. **539**, L41 (2000).
[5] M. S. Turner *et al.*, *Connecting Quarks with the Cosmos* (National Academies Press, Washington, DC, 2003).
[6] G. X. Chen, K. Kirby, E. Silver, N. S. Brickhouse, J. D. Gillaspy, J. N. Tan, J. Pomeroy, and J. M. Laming, Phys. Rev. Lett. **97**, 143201 (2006).
[7] G. V. Brown, P. Beiersdorfer, D. A. Liedahl, and K. Widmann, Astrophys. J. **502**, 1015 (1998); J. M. Laming *et al.*, Astrophys. J. Lett. **545**, L161 (2000).
[8] G. X. Chen and A. K. Pradhan, Phys. Rev. Lett. **89**, 013202 (2002); G. X. Chen, A. K. Pradhan, and W. B. Eissner, J. Phys. B **36**, 453 (2003).
[9] P. Beiersdorfer, Annu. Rev. Astron. Astrophys. **41**, 343 (2003).
[10] T. R. Kallman and P. Palmeri, Rev. Mod. Phys. **79**, 79 (2007).
[11] D. E. Osterbrock, *Astrophysics of Gaseous Nebulae and Active Galactic Nuclei* (University Science Books, New York, 1989).
[12] J. N. Reeves *et al.*, Nature (London) **416**, 512 (2002); Y. Krongold *et al.*, Astrophys. J. **597**, 832 (2003).
[13] R. K. Smith, N. S. Brickhouse, D. A. Liedahl, and J. C. Raymond, Astrophys. J. **556**, L91 (2001).
[14] G. V. Brown *et al.*, Phys. Rev. Lett. **96**, 253201 (2006).
[15] H. L. Zhang and D. H. Sampson, At. Data Nucl. Data Tables **43**, 1 (1989).
[16] K. A. Berrington, W. Eissner, and P. H. Norrington, Comput. Phys. Commun. **92**, 290 (1995).
[17] K. M. Aggarwal, F. P. Keenan, and A. Z. Msezane, Astrophys. J., Suppl. Ser. **144**, 169 (2003); K. M. Aggarwal, F. P. Keenan, and R. Kisielius, Astron. Astrophys. **420**, 783 (2004).
[18] S. D. Loch, M. S. Pindzola, C. P. Ballance, and D. C. Griffin, J. Phys. B **39**, 85 (2006).
[19] K. B. Fournier and S. B. Hansen, Phys. Rev. A **71**, 012717 (2005).
[20] F. A. Parpia, C. F. Fischer, and I. P. Grant, Comput. Phys. Commun. **94**, 249 (1996).
[21] P. H. Norrington and I. P. Grant, J. Phys. B **20**, 4869 (1987); S. Ait-Tahar, I. P. Grant, and P. H. Norrington, Phys. Rev. A **54**, 3984 (1996).
[22] M. Mohan, R. Sharma, and W. Eissner, Astrophys. J., Suppl. Ser. **108**, 389 (1997).
[23] J. H. Scofield, J. Electron Spectrosc. Relat. Phenom. **8**, 129 (1976); Phys. Rev. A **40**, 3054 (1989).
[24] http://physics.nist.gov/PhysRefData/.